REPORT DOCUMENTATION PAGE

Form Approved OMB NO. 0704-0188

1. AGENCY USE ONLY (Leave Blank)	2. REPORT DATE:	3. REPORT TYPE AND DATES COVERED Final Report 1-Sep-2002 - 31-Aug-2005

4. TITLE AND SUBTITLE

Nanoscale Characterization of Failure Processes in Polymer Nanocomposites

5. FUNDING NUMBERS

DAAD190210332

6. AUTHORS

Raman P. Singh

8. PERFORMING ORGANIZATION REPORT NUMBER

7. PERFORMING ORGANIZATION NAMES AND ADDRESSES

State University of New York at Stony Broo
Office of Sponsored Programs
Research Foundation Of SUNY
Stony Brook, NY 11794 -3362

9. SPONSORING/MONITORING AGENCY NAME(S) AND ADDRESS(ES)

U.S. Army Research Office
P.O. Box 12211
Research Triangle Park, NC 27709-2211

10. SPONSORING / MONITORING AGENCY REPORT NUMBER

44035-EG.1

11. SUPPLEMENTARY NOTES

The views, opinions and/or findings contained in this report are those of the author(s) and should not contrued as an official Department of the Army position, policy or decision, unless so designated by other documentation.

12. DISTRIBUTION AVAILIBILITY STATEMENT

Approved for Public Release; Distribution Unlimited

12b. DISTRIBUTION CODE

13. ABSTRACT (Maximum 200 words)

The abstract is below since many authors do not follow the 200 word limit

14. SUBJECT TERMS

nanoindentation, polymer, viscoelastic, fracture, acoustic emission

15. NUMBER OF PAGES

Unknown due to possible attachments

16. PRICE CODE

17. SECURITY CLASSIFICATION OF REPORT	18. SECURITY CLASSIFICATION ON THIS PAGE	19. SECURITY CLASSIFICATION OF ABSTRACT	20. LIMITATION OF ABSTRACT
UNCLASSIFIED	UNCLASSIFIED	UNCLASSIFIED	UL

Report Title

Nanoscale Characterization of Failure Processes in Polymer Nanocomposites

ABSTRACT

This project was focussed on two areas of investigation: application of novel displacement modulation techniques for nanoindentation based viscoelastic characterization; and the use of acoustic emission
characterize nanoindentation induced fracture in brittle materials and advanced. A new displacement modulation technique has been developed and employed for determining the storage and loss moduli of viscoelastic polymers, as a function of frequency. This new technique represents a highly superior approach in comparison will all other existing techniques for dynamic indentation. Acoustic emission sensing has been established as a robust technique for quantifying failure in brittle materials, advanced ceramics and a new type of amorphous ceramic material. Collaboration with various researchers at the US Army Research Labororatory at Aberdeen Proving Ground provided fruitful benefits.

List of papers submitted or published that acknowledge ARO support during this reporting period. List the papers, including journal references, in the following categories:

(a) Papers published in peer-reviewed journals (N/A for none)

Dyjak, P., and R. P. Singh, "Acoustic Emission Analysis of Nanoindentation-Induced Fracture Events," Experimental Mechanics, in press, 2006.

Number of Papers published in peer-reviewed journals: 1.00

(b) Papers published in non-peer-reviewed journals or in conference proceedings (N/A for none)

Singh, R. P., S. P. Singh and J. F. Smith, "Displacement Modulation Based Dynamic Nanoindentation for Viscoelastic Material Characterization," Fundamentals of Nanoindentation and Nanotribology III, edited by Kathryn J. Wahl, Norbert Huber, Adrian B. Mann, David F. Bahr, and Y.-T. Cheng, Materials Research Society Symposium Proceedings, Vol. 841, Paper No. R4.6, Warrendale, Pennsylvania, 2005.

Dyjak, P., and R. P. Singh, "Acoustic Emission Analysis of Nanoindentation-Induced Fracture Events," Fundamentals of Nanoindentation and Nanotribology III, edited by Kathryn J. Wahl, Norbert Huber, Adrian B. Mann, David F. Bahr, and Y.-T. Cheng, Materials Research Society Symposium Proceedings, Vol. 841, Paper No. R8.10, Warrendale, Pennsylvania, 2005.

Number of Papers published in non peer-reviewed journals: 2.00

(c) Papers presented at meetings, but not published in conference proceedings (N/A for none)

Dyjak, P., and R. P. Singh, "Investigation of Nanoindentation Induced Fracture in Brittle Materials," SEM Annual Conference and Exposition on Experimental and Applied Mechanics, Portland, Oregon, June 7 - 9, 2005.

Singh, S. P., and R. P. Singh, "Displacement Based Characterization of Viscoelastic Materials Using Dynamic Indentation," SEM Annual Conference and Exposition on Experimental and Applied Mechanics, Portland, Oregon, June 7 - 9, 2005.

Singh, R. P., S. P. Singh and J. F. Smith, "Displacement Modulation Based Dynamic Nanoindentation for Viscoelastic Material Characterization," Symposium R, Fundamentals of Nanoindentation and Nanotribology III, MRS Fall Meeting, Boston, Massachusetts, November 29 - December 3, 2004.

Singh, R. P, M. R. VanLandingham and P. L. Drzal, "Comparative Evaluation of Different Dynamic Nanoindentation Techniques Used for Testing Polymeric Materials," Symposium R, Fundamentals of Nanoindentation and Nanotribology III, MRS Fall Meeting, Boston, Massachusetts, November 29 - December 3, 2004.

Dyjak, P., and R. P. Singh, "Acoustic Emission Analysis of Nanoindentation-Induced Fracture Events," Symposium R, Fundamentals of Nanoindentation and Nanotribology III, MRS Fall Meeting, Boston, Massachusetts, November 29 - December 3, 2004.

Dyjak, P., and R. P. Singh, "Acoustic Emission Analysis of Nanoindentation-Induced Fracture Events," 15th International Invitational Symposium on the Unification of Analytical, Computational, and Experimental Solution Methodologies in MEMS and Nanotechnology (UACEM) Symposium, Springfield, Massachusetts, October 27 - 29, 2004.

Singh, S. P, and R. P. Singh, "Characterization of Viscoelastic Behavior of Polymers using Dynamic Nanoindentation," 15th International Invitational Symposium on the Unification of Analytical, Computational, and Experimental Solution Methodologies in MEMS and Nanotechnology (UACEM) Symposium, Springfield, Massachusetts, October 27 - 29, 2004.

Singh, S.P, and R.P. Singh, "Use of Nanoindentation to Measure the Complex Modulus Behavior of Polymers," Graduate Student Symposium on Mechanics and Packaging, Worcester Polytechnic Institute, Worcester, Massachusetts, May 2004.

Number of Papers not Published: 8.00

(d) Manuscripts

Singh, S. P., R. P. Singh and J. F. Smith, "Viscoelastic Characterization of Polymers Using a Displacement Modulation Based Dynamic Indentation Method." Experimental Mechanics, under review, 2006.

Singh, S. P., Singh, R. P., and Smith, J., “Use of Nanoindentation For Complex Compliance Measurements On Polymers, Manuscript under preparation. Targeted submission: Review of Scientific Instruments (2006).

Number of Manuscripts: 2.00

Number of Inventions:

Graduate Students

NAME	PERCENT_SUPPORTED	
Pawel Dyjak	1.00	No
Sehaj P. Singh	1.00	No
Yuqin Liu	0.50	No
FTE Equivalent:	**2.50**	
Total Number:	**3**	

Names of Post Doctorates

NAME	PERCENT_SUPPORTED
FTE Equivalent:	
Total Number:	

Names of Faculty Supported

NAME	PERCENT_SUPPORTED	National Academy Member
Raman P. Singh	0.33	No
FTE Equivalent:	**0.33**	
Total Number:	**1**	

Names of Under Graduate students supported

NAME	PERCENT_SUPPORTED
FTE Equivalent:	
Total Number:	

Names of Personnel receiving masters degrees

NAME	
Pawel Dyjak (2005)	No
Yuqin Liu (Expected 2006)	No
Total Number:	**2**

Names of personnel receiving PHDs

NAME	
Sehaj P Singh (Expected 2006)	No
Total Number:	**1**

Names of other research staff

NAME	PERCENT_SUPPORTED
FTE Equivalent:	
Total Number:	

Sub Contractors (DD882)

Inventions (DD882)

Final Progress Report

Proposal Number: 44035EG
Agreement Number: DAAD190210332
Nanoscale Characterization of Failure Processes in Polymer Nanocomposites

September 1, 2002–August 31, 2005

Raman P. Singh*
Mechanics of Advanced Materials Laboratory
Department of Mechanical Engineering
Stony Brook University
Stony Brook, NY 11794, USA

*Corresponding author: raman.singh@sunysb.edu (email)

Contents

List of Figures

List of Tables

1 Acoustic Emission Analysis of Nanoindentation Induced Fracture Events

Abstract

Monitoring of acoustic emission activity is employed to characterize the initiation and progression of local failure processes during nanoindentation-induced fracture. Specimens of various brittle materials are loaded with a cube-corner indenter and acoustic emission activity is monitored during the entire loading and unloading event using a transducer mounted inside the specimen holder. As observed from the nanoindentation and acoustic emission response, there are fundamental differences in the fracture behavior of the various materials. Post-failure observations are used to identify particular features in the acoustic emission signal that correspond to specific types of fracture events. Furthermore, analysis of the parametric and transient acoustic emission data is used to establish the crack-initiation threshold, crack-arrest threshold, and energy dissipation during failure. It is demonstrated that the monitoring of acoustic emission signals yields both qualitative and quantitative information regarding highly localized failure events in brittle materials.

1.1 Introduction

Nanoindentation, also known as ultra-low load indentation, is a powerful technique for characterizing the mechanical properties of materials at very small length scales [1, 2, 3]. In this technique, a well-defined diamond tip is indented into the material of interest while the applied load and displacement are continuously monitored during one complete loading and unloading cycle. Current nanoindentation systems can typically provide resolutions of 1 nN and 0.1 nm for force and displacement measurements, respectively, which enable the mechanical sampling of very small material volumes. Typically, nanoindentation has been employed to determine hardness and elastic modulus [2], but it can also be used to determine the fracture toughness of brittle materials [4]. When a brittle material is loaded by a sharp indenter, radial cracks propagate out of the indenter corners if a sufficiently large load is applied, as shown in Fig. 1. In such a case the fracture toughness can be estimated by measuring the length of radial cracks produced at a given indentation load [5]. This procedure has proved to be adequate for

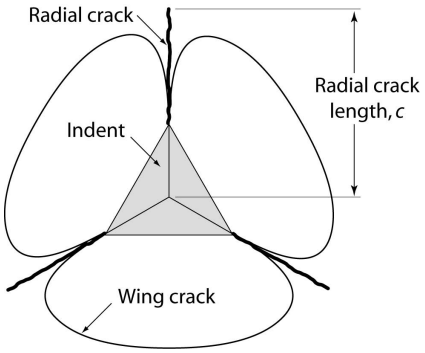

Figure 1: Top view of the radial and wing crack fracture pattern resulting from an indentation.

providing an averaged measure of fracture toughness in homogeneous materials. However, it provides no information regarding the crack initiation and growth. Furthermore, this technique cannot delineate energy dissipation by various fracture processes that occur for a locally heterogeneous material. Additionally, the need for measuring the crack length after each test impedes the calculations of fracture toughness. Appropriate identification of the events during crack initiation and growth is an essential step towards characterizing the overall failure behavior of locally heterogeneous materials using nanoindentation. Fortuitously, failure events in brittle materials are accompanied by abrupt changes in stress and strain fields, which lead to the generation of transient elastic waves in the form of acoustic emission. The real-time monitoring of acoustic emission can then be used as a qualitative and quantitative diagnostic tool [6, 7, 8]. This paper reports on the use of high resolution acoustic emission sensing to monitor nanoindentation induced fracture and characterize the initiation and progression of local failure processes.

1.2 Experimental details

1.2.1 Indentation and acoustic emission setup

Specimens of various brittle materials were loaded with a cube-corner indenter in a NanoTest instrument (Micro Materials Ltd., Wrexham, United Kingdom). Currently available nanoindentation systems have limited acoustic emission monitoring capability, if any. Therefore a custom system was

designed and implemented by retrofitting the NanoTest instrument with a standalone acoustic emission monitoring system (AMSY-5, Vallen-Systeme GmbH, Munich, Germany). The nanoindentation setup has a unique pendulum design, as shown in Fig. 2, with the pendulum pivoted at approximately midpoint. The load is applied through an electromagnetic transducer at the

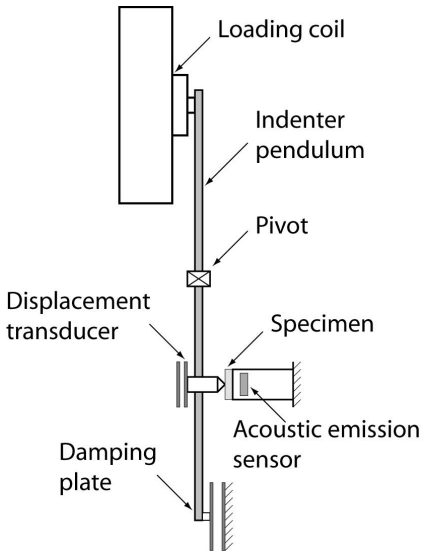

Figure 2: Schematic of the Nanotest platform showing the incorporation of an acoustic emission sensor in the specimen holder.

top of the pendulum and is transferred to the other end, which has the indenter in contact with the sample. The displacement of the diamond indenter tip is measured by means of a parallel plate capacitor, one plate of which is attached to the indenter holder; when the indenter moves, the capacitance changes, and this is measured by means of a capacitance bridge. The capacitance bridge unit is located close to the measuring capacitor in order to minimize stray capacitance effects. A cube-corner indenter was chosen due to its geometry; a three-sided pyramid with mutually perpendicular faces arranged in a geometry like the corner of a cube. The centerline-to-face angle for this indenter is 34.3, whereas for the Berkovich indenter it is 65.3. The sharper cube corner produces much higher stresses and strains in the vicinity of the contact, which reduces the fracture threshold load. This is useful, in producing very small, well-defined cracks around indents in brittle materials; such cracks can then be used to estimate the fracture toughness at rela-

tively small scales [9]. The acoustic emission activity was monitored with AMSY-5, which can store more than 30,000 AE-hits/s and more than 2.5 MBytes/s of waveform data, filtered and time sorted in real time to the hard drive. The unit is also capable of recording data on two parametric channels; data such as environmental conditions as well as the external load as reference parameters for the detected acoustic emission. The AMSY-5 captures the elastic waves propagating through the material and converts them into the electrical signals by the acoustic emission sensors. Piezo-electric sensors have proved to be most appropriate for all types of acoustic emission testing. They are robust and extremely sensitive. The optimal frequency range to be chosen depends on the expected kind of acoustic emission sources and the conditions of wave propagations, wave attenuation and distances. For the purpose of this investigation, the employed transducer had a frequency response in the range of 100 to 400kHz (AE104A, Vallen-Systeme GmbH, Munich, Germany). The signal, received by the sensor, is then fed electrically to the 34dB gain preamplifier, with a wideband response from 2.5kHz to 3MHz. The signal from the preamplifier is then received in the acoustic signal preprocessor (ASIPP) and converted into a digital data stream. The acoustic emission features such as time of the first threshold crossing, rise time, duration time, peak amplitude, energy and counts are then extracted by a field programmable gate array (FPGA) on the ASIPP. This data, along with the parametric data is then transferred to the acoustic emission system controller (AsyC) where all the data is assembled into data sets. All data sets are temporarily stored in the memory of the AsyC and then transferred to a file on the PC hard disk under control of the acquisition program. In parallel to the assembling and transferring of the acoustic emission data the AsyC reads the waveform data from the ASIPPs transient recorder and transfers it to the file on the PC hard disk. Acoustic emission activity was monitored during the entire loading and unloading event using a transducer mounted inside the specimen holder. By locating the acoustic emission sensor directly underneath the sample it was possible to eliminate spurious signals that may occur when the diamond indenter is not effectively coupled with the sample [10]. Acoustic emission signals were recorded and correlated with the nanoindentation data in real time, using the following parameters: threshold value of 21.9dB, transient sampling rate of 10 MHz and parametric timing of 0.001s. A typical transient acoustic emission waveform from an indentation induced fracture event can be broken down into a set of parameters such as the number of counts, energy, rise time, duration time and peak amplitude,

as shown in Fig. 3. The number of counts being the number of times the

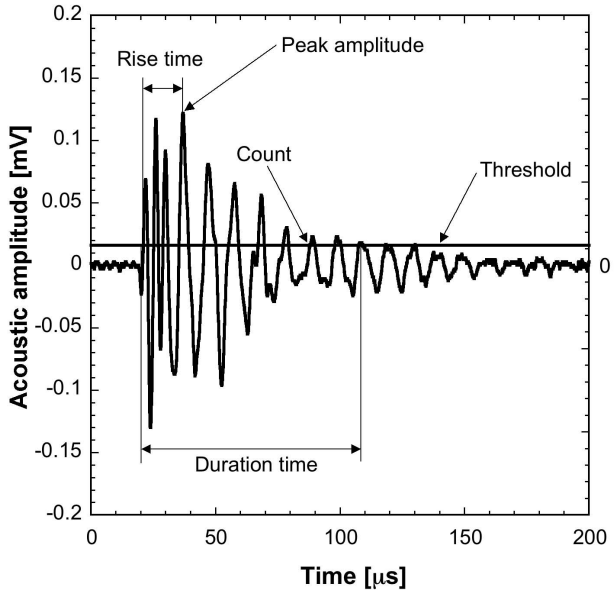

Figure 3: Full transient acoustic emission waveform.

signal crosses the threshold value. The energy is the integral of the squared of the amplitude over the signal duration. The rise time is the time between the first threshold crossing and peak amplitude. The duration is the time between the first and last threshold crossing. This paper is focused on these parameters rather than on the entire transient acoustic emission waveform. The statistical evaluation of waveforms is more difficult than that of certain waveform features and will be the focus of future work since it can conceivably provide more information. The nanoindentation and acoustic emission detection systems were integrated to provide a common time base for direct comparison of data. Since the nanoindentation system is separate from the acoustic emission detection system two separate computers are necessary to record the data during an experiment. To superimpose the two data sets, a common time frame was obtained by recording the displacement voltage from the indenter using a parametric input on the acoustic emission detection system. Since the maximum recorded parametric voltage corresponded to the maximum depth during the indentation process, a common timeframe was thus established. The flowchart, Fig. 4, shows the two processes running in parallel and the open dashed arrow indicates the synchronization step. The

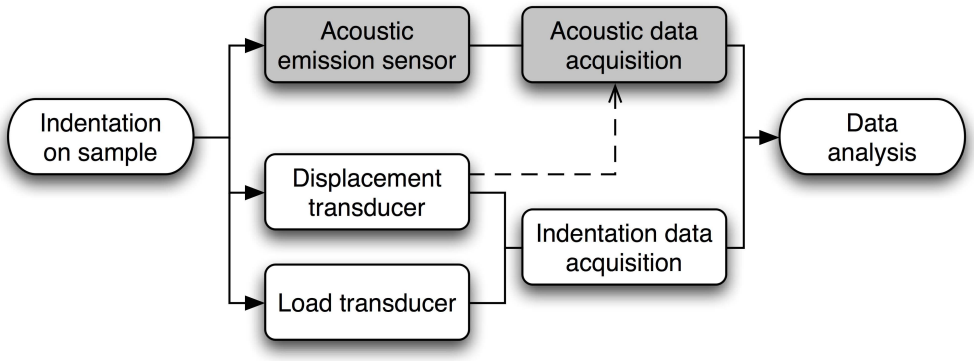

Figure 4: Block diagram of the acoustic emission and indentation signal.

identification of appropriate settings, especially threshold, was achieved by extensive characterization of noise levels and testing on aluminum as a reference material. The initial experiments were done with a very low acoustic emission sensitivity threshold level of 9.9dB, as to not miss any acoustic emission events. This however proved to be not the optimal scenario since there were many events with very low amplitudes detected. These acoustic emission hits were present even when the indentation was not taking place and the acoustic emission sensor was detecting ambient noise [11]. To remedy the situation the threshold setting was raised to 21.9dB. This value was determined experimentally by indenting on an aluminum specimen. Since aluminum is not a brittle material it should not exhibit nanoindentation induced fracture and any associated acoustic emission activity. Therefore, tests conducted on aluminum were used to evaluate the validity of the selected acoustic emission setting and filters. Fig. 5 shows the indentation load-depth data and the associated acoustic emission data for experiments conducted on aluminum. During the loading part of the indentation there were no acoustic emission events and only three hits occurred during the unloading cycle. Since only few events were recorded this confirmed that an appropriate setting for the acoustic threshold value had been selected. Furthermore, at lower threshold values the acoustic emission sensor detected considerable machine noise and ambient vibrations.

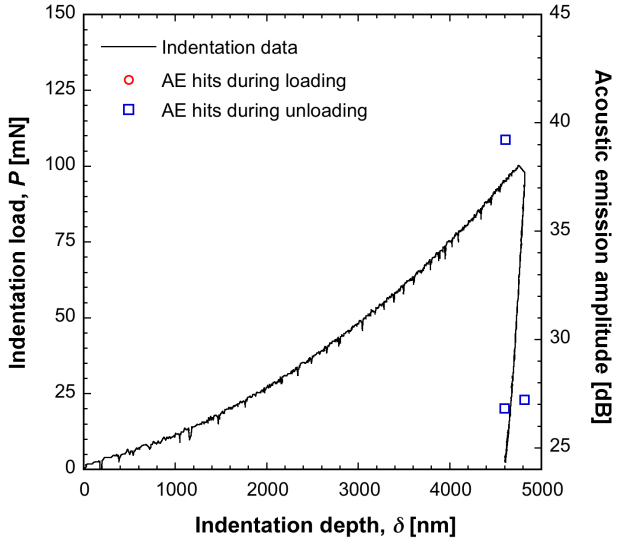

Figure 5: Load-displacement and acoustic emission data on an aluminum specimen.

1.2.2 Materials and testing procedure

Indentation fracture experiments were carried out at various loads including 25 mN, 125 mN, 225 mN, 250 mN and 450 mN for both single loading, and multiple loading-unloading conditions. The multiple loading-unloading tests were performed to clearly relate the acoustic emission activity to the fracture process. It is conceivable that friction/slipping along the indenter faces could also lead to the generation of acoustic emissions. The multiple loading-unloading tests served as a test to ensure that acoustic emission activity during an experiment corresponds only to fracture and no other spurious events. In these experiments, the sample was loaded to the initial maximum load and then unloaded to 15% of the maximum load value and then loaded again to the next peak load. This was repeated until the maximum load for the entire experiment was achieved. Three loading-unloading cycles were used during each of the repeated load experiments. The partial unloading eliminated any alignment issues for the successive indentation as well as prevented debris from falling into the indentation. The procedure was employed to test three different materials including soda lime glass, a beta crystalline silicon carbide (Rohm and Haas Co., Woburn, Massachusetts)

and glass-ceramic (Macor, Corning Inc., Corning, New York). Table 1 shows various material properties of the above mentioned materials such as Youngs modulus, Poissons ratio, bulk fracture toughness from literature, and density.

Property	**Glass**	**SiC**	**Macor**	**Aluminum**
Elastic Modulus [GPa]	70.3	466	66.9	69
Poisson's ratio	0.22	0.21	0.29	0.33
Fracture toughness [MPa·m$^{1/2}$]	0.75	3.3	1.53	29
Density [g/cm^3]	2.47	3.21	2.52	2.70

Table 1: Properties of materials tested for nanoindentation induced fracture

The soda lime glass was chosen as it represents a brittle material with a glassy/amorphous microstructure. In contrast to the other materials, glass offered a comparison to more complex microstructures. The beta crystalline silicon carbide had a face centered cubic polycrystalline microstructure with the grain size between 5 to 10 microns. The high purity chemical vapor deposition manufacturing process ensured a very pure specimen (>99.9995% SiC) which made for very good repeatability. The cubic beta structure offered isotropic characteristics, which simplified the experimental setup since the spatial orientation of the specimen was not crucial. The Macor is different from the other materials and represents a heterogeneous composite. It is a machinable glass ceramic material composed of approximately 55% fluorophlogopite mica and 45% borosilicate glass. This makes for a rather complex microstructure due to the presence of the mica reinforcements. The fracture toughness of Macor and SiC were 2 and 4 times as great as that of glass, respectively. All of the specimens were cut to the size 12mm x 12mm x 3mm. The soda lime glass did not require any surface treatment since a high surface finish microscope slide was used as the starting material. The Macor and SiC specimen were cut using a diamond wheel saw and polished using 3μm diamond slurry and 0.05μm colloidal alumina to achieve very low surface roughness. After the samples were sufficiently polished they were mounted on a specially designed specimen holder which encased the acoustic emission sensor. The tip of the sensor was flushed with the top surface of the holder and silicone grease was applied to ensure good coupling. The samples were then held in place with cyanoacrylate adhesive.

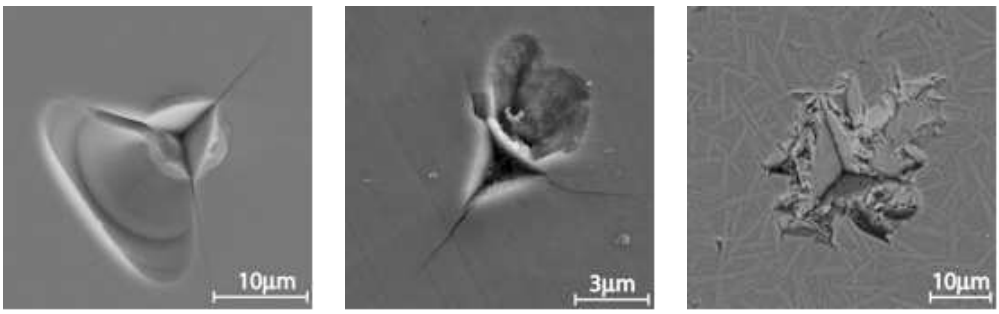

(a) (b) (c)

Figure 6: Cube corner indentation of (a) glass, (b) beta crystalline silicone carbide, and (c) Macor.

1.3 Results and discussion

1.3.1 Fracture detection by acoustic emission and threshold load

Fig. 6 shows the scanning electron microscope (SEM) images of nanoindentation induced cracks in the three materials that were tested; soda lime glass, silicon carbide and Macor. Each of the tested materials exhibited unique fracture processes. These failure processes are better understood by examining the nanoindentation data and acoustic emission activity in conjunction with the SEM micrographs. Figure 7 shows typical indentation load-depth data and the associated acoustic emission data for fracture experiments conducted on glass and silicon carbide.

From just the indentation data it is not possible to identify whether any fracture events have taken place. The load-depth curves are smooth and do not exhibit any abrupt changes in slope that may indicate sudden changes in contact compliance occurring due to localized fracture. However, SEM images taken at the end of the experiment clearly show that fracture occurred by the formation of both radial and wing cracks, as indicated in Fig. 6 (a) and (b) for glass and silicon carbide, respectively. In contrast, the acoustic emission data provides a real-time visualization of the nanoindentation induced fracture process. The acoustic emission data is superimposed on the load-depth curve by establishing a common time base as discussed earlier. The acoustic emission data provides additional information about the local fracture processes. There appears to be no detectable acoustic emission activity until a certain indentation load is reached, as shown in Fig. 7. After

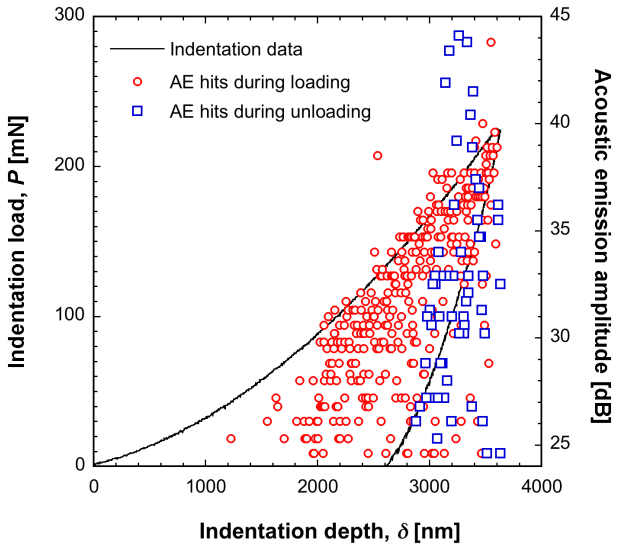

(a)

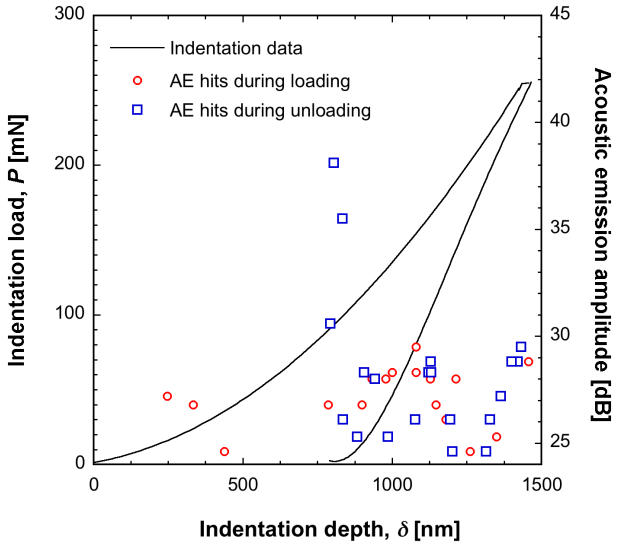

(b)

Figure 7: Load-displacement and acoustic emission data obtained from fracture experiments conducted on (a) glass and (b) silicon carbide.

this occurs, the acoustic emission activity is much more frequent. The examination of several indentation experiments led to the observation that this phenomenon always occurred at a very similar load for a given material. To avoid any spurious acoustic emission events from affecting the determination of this load the acoustic emission energy was used to determine the threshold load, since the energy can provide more information about the intensity of the hit. The energy distinguishes itself from amplitude because it also contains information about the duration of the hit. Although similar duration information could be gained from counts, the energy data should have better resolution. As shown in Fig. 8 (a), when cumulative energy is plotted as a function of time, changes in slope can be seen.

The test was load controlled and after the peak load was reached there is a dwell period of 10 seconds, where the load should remain constant unless the contact compliance changes and the indenter cannot move fast enough to compensate. However, the contact compliance keeps reducing due to continuation of the fracture process. Thus the indenter is driven further and further into the material in order to maintain constant load. But the machine is not fast enough to do this (in keeping with the fracture process), and hence the load decreases, the depth increases, and the acoustic emission activities accumulates. The acoustic emission changes, only after the unloading cycle starts. The second change in slope may correspond to the initiation of the wing cracks. The details of the change in slope are shown in Fig. 8 (b). It is right at this change in slope that the crack initiation threshold occurs. Similarly the change in slope can be seen in silicon carbide as shown in Fig. 9.

For the case of glass, after the threshold load for glass is exceeded, the acoustic emission activity appears to be continuous with lower amplitudes during the loading cycle and higher amplitudes during the unloading cycle. The continuous acoustic emission implies that the crack growth is continuous as well, which would be consistent with the amorphous microstructure of soda lime glass. During the loading segment the amplitudes are also continuously increasing proportionally to the indentation load. The amplitudes of the acoustic emission may be directly proportional to the surface area of the propagating crack, but the actual depth of the cracks is difficult to estimate without examining the cross sectional view or making several assumptions, therefore a detailed relationship with the crack surface area is not examined in this paper. The appearance of acoustic emission activity during both loading and unloading can be understood in terms of the formation of radial and

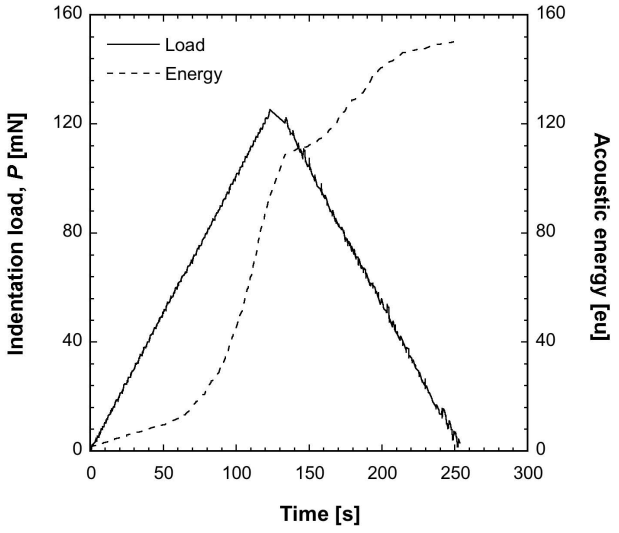

(a)

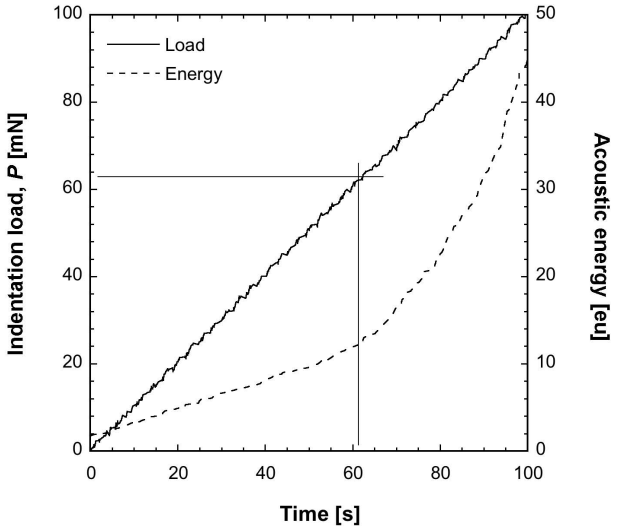

(b)

Figure 8: Determination of crack threshold load on a glass specimen using the change in slope of the acoustic energy (a) view of the entire experiment, (b) details of the change of slope.

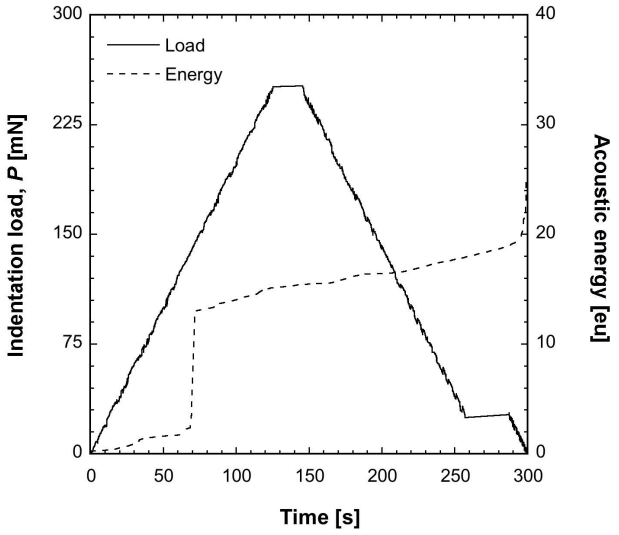

(a)

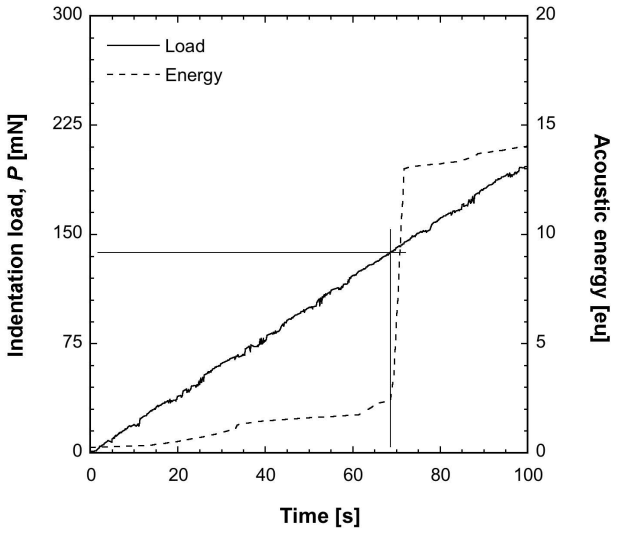

(b)

Figure 9: Determination of crack threshold load on a silicon carbide specimen using the change in slope of the acoustic energy (a) view of the entire experiment, (b) details of the change of slope.

wing cracks during the indentation of a brittle material. The entire process of crack formation begins with the indenter contacting and penetrating the specimen surface. The loading process leads to the direct formation of radial cracks that radiate out from all corners of the indent. The penetration of the indenter also leads to a plastically deformed zone surrounding the indentation site and gives rise to tensile zones adjacent to the contact as well as a sub-surface tensile stress field immediately beneath the indenter tip [12, 13, 14]. The penetration may also produce a median vent right under the indenter tip. Further loading results in the sub-surface median vent being able to break through the specimen surface. Upon unloading, debris and plastic-elastic mismatch, prevent the median vents from closing up leading to the formation of lateral cracks, starting from the center of the indentation and moving in the radial outward direction, parallel to the specimen surface [15]. These cracks may continue to grow even after the removal of the indenter and that is one of the reasons why the acoustic emission sensor was placed on the specimen rather than on the indenter tip. Provided that high enough loads are applied, these lateral cracks may intersect the specimen surface, after which they are termed as wing cracks [12, 13, 14]. Since it is believed that the radial cracks are formed during loading and wing cracks are formed during the unloading it is likely that the lower amplitude signals, during loading, are linked to the growth of radial cracks and the higher amplitude signals, during unloading, are linked to the growth of wing cracks. During unloading the amplitudes may be higher since more fracture surface area is created through the formation of the wing crack, rather than the radial crack, leading to higher energy/amplitude acoustic events during unloading. However both radial and wing cracking mechanisms occurring in a continuous fashion are linked to the glass being brittle and having an amorphous microstructure. Silicon carbide showed a completely different fracture process. Although the SEM image shows a radial crack pattern similar to that of glass, the crystalline structure affected both the radial and wing crack formation. The total number of acoustic emission events was much lower than that for glass and instead of continuous crack formation the acoustic emission signals were highly discrete. There were a few discrete acoustic emission signals during the loading cycle, followed by a higher rate of large amplitude signals at the very end of the unloading cycle. The discrete signals, during loading, imply crack growth in short bursts rather than a continuous fashion as for glass. Furthermore, the duration times of the acoustic emission events for silicon carbide were shorter than that of glass further implying short, intermittent

and perhaps faster crack growth. However, direct comparison of amplitudes between glass and silicon carbide is not applicable due to differences in acoustic impedance. The fracture threshold values, as determined by the onset of acoustic emission activity, are listed in Table refthreshold for the three materials. The table also lists the values of average fracture toughness, K_{Ic},

Property	**Glass**	**SiC**	**Macor**
Threshold load [mN]	60 ± 9	171 ± 22	43 ± 21
Indentation fracture toughness [MPa·m$^{1/2}$]	0.53	3.23	N/A

Table 2: Threshold load values for acoustic emission activity and indentation fracture toughness

determined by measuring the radial crack length and the peak load [5]:

$$K_{Ic} = \alpha(\frac{E}{H})^{1/2}\frac{P}{c^{3/2}}, \tag{1}$$

where α is a constant dependent on the geometry of the indenter (α= 0.04 for cube-corner), E is the Youngs modulus, H is the hardness, P is the maximum indentation load and c is the radial crack length. The formula for fracture toughness by indentation has been derived assuming that the radial cracks produced at corners of the indent are long [5]. In the experiments with glass and silicon carbide long radial cracks are present. These two materials also show direct correspondence between the K_{Ic} and the threshold load for acoustic emission activity. Therefore the threshold loads serve as a direct indicator of the fracture toughness. However this is not the case for Macor which did not exhibit clearly defined, long radial cracks, as discussed later.

1.4 Classification of the failure process by the energy of acoustic emission

The acoustic emission data can be analyzed further to quantify the fracture process. By examining the energy parameter it is possible to establish a clear relationship between the acoustic emission energy during the loading cycle and the length of the radial cracks for both glass and silicon carbide, as shown in Fig. 10.

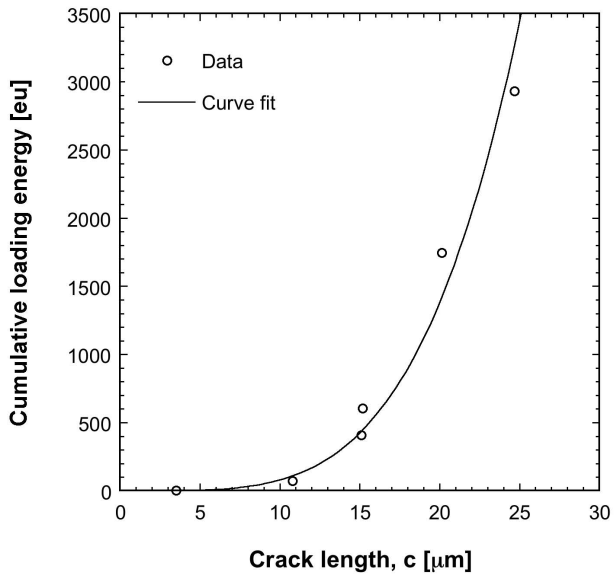

(a)

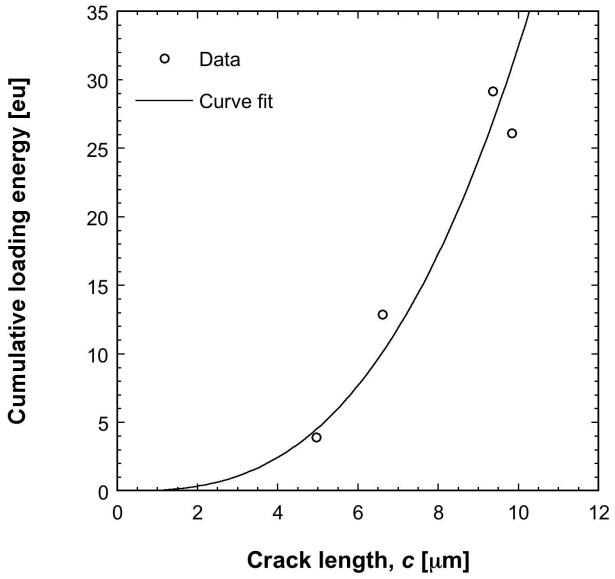

(b)

Figure 10: Cumulative acoustic emission energy during loading for (a) glass and (b) silicon carbide.

Note that each data point in these plot represents a separate experiment. For the case of glass, the best fit was achieved using

$$AE\ energy = 0.007c^{4.1}, \tag{2}$$

where c is the radial crack length. Similarly, for silicon carbide

$$AE\ energy = 0.202c^{2.1}, \tag{3}$$

For silicon carbide the energy was proportional to the area swept by the radial cracks, which confirms the results of Bahr and Gerberich [16, 17]. However, this is not the case for glass and could be due to the amorphous microstructure. In both materials this correlation allows the determination of the crack lengths from the acoustic emission energy and thus the real-time calculation of fracture toughness, without the requirement to measure radial crack lengths using post- experiment microscopy. The ability to continuously monitor cumulative acoustic emission energy also allows for the determination of crack growth, once the specific energy crack length relationship has been established for a particular material. Since it is believed that the wing cracks occur during the unloading of the material, the unloading acoustic emission energy should correlate to the wing crack area after completing the indentation. Such a relationship was observed for silicon carbide, where the energy was found to be linearly proportional to the area of the wing crack. Table 3 shows the coefficient of correlation (R2) between the unloading/loading energy and wing/radial crack area/length.

Fracture feature	**AE energy loading**	**AE energy unloading**
Radial crack lengths squared	0.963	0.073
Wing crack area	0.678	0.869

Table 3: Correlation coefficient (R2) values for silicon carbide

The loading energy correlates very well with the radial crack length and unloading energy correlates very well with the wing crack area and not vice versa. These measurements provide direct experimental validation of the mechanistic postulate that radial cracks are generated during the loading process and wing cracks during unloading.

1.4.1 Failure and acoustic emission in a heterogeneous ceramic

The third material tested, Macor, shows a different fracture mechanism due to its heterogeneous microstructure. As shown by the load and depth versus time indentation curve in Fig. 11, there are distinct regions in which the indentation depth increases very suddenly at almost constant indentation load. These experiments are conducted in a load-controlled mode.

Thus these regions correspond to drastic loss in contact compliance, which most likely correspond to the material undergoing some failure process. Furthermore, the increases do not occur at the same loads and they vary from experiment to experiment, which implies that the failure process is being governed by the locally random microstructure at the indentation location. Since Macor is composed of approximately 55% fluorophlogopite mica and 45% borosilicate glass; these mica reinforcements are directly responsible for the sudden increases in the indentation depth. The cracks in the material grow until they are arrested by these randomly oriented reinforcements. The growth of these cracks is possibly accompanied with material removal by a chipping process. Once material removal occurs by one such chipping process, no further increase in load is observed until the indenter penetrates deeper. The process is periodically repeated, as illustrated in Fig. 11 (a) where three distinct sudden increases in indentation depth. The acoustic emission data is consistent with the observations discussed above. Initially there is no acoustic emission activity until a certain threshold load is reached at about 43 mN. This load was determined using the cumulative acoustic energy technique described in the prior sections. The acoustic emission amplitudes increase proportionally to the load applied until they reach the highest value at the moment of the sudden increase in depth at constant load. Fig. 11 (b) shows the details of one such sudden increase in the indentation depth. The corresponding acoustic emission hits have typically higher amplitudes and occur at much higher rates as illustrated in Fig. 12. The depth of the indentation rapidly increases until the growth of the fracture pattern is stopped by the crack tips arresting at the mica reinforcements and further penetration by the indenter. In order for the crack to grow further, since it cannot go through the reinforcements; it has to go around it, thus requiring more energy. Therefore, less acoustic emission activity is observed until the indentation load has increased sufficiently to repeat the fracture process. No radial cracks were discovered after examining the indents, therefore the acoustic emission energy cannot be correlated to the radial crack

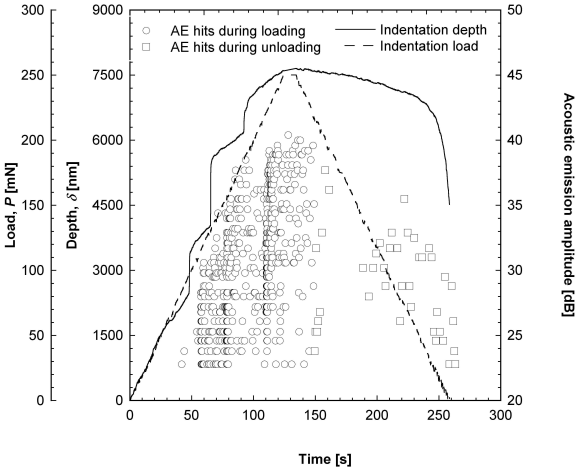

(a)

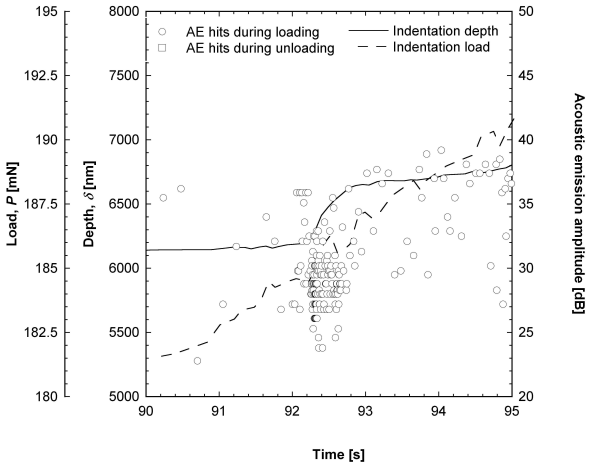

(b)

Figure 11: Macor (a) Load, displacement and acoustic emission data, (b) details of the sudden increase in depth.

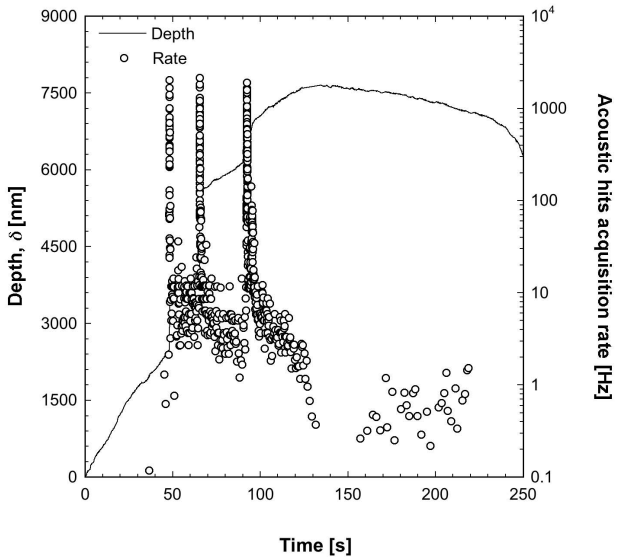

Figure 12: Rate of acquisition of acoustic emission hits in Macor.

length. However the acoustic emission energy can be correlated to the area of the fracture zone. From Fig. 13 it can be seen that the acoustic energy is logarithmically proportional to the projected area of the fracture zone and the best fit is achieved using

$$AE\ energy = 1.355e^{0.0133A}, \tag{4}$$

where A is the area of the fracture zone.

This information is not directly applicable for calculating the fracture toughness of the Macor material, but enables some quantitative damage approximation. The acoustic emission energy may be more closely related to the volume of the removed material. Since it is difficult to quantify the volume of the removed material without making several assumptions about the depth of the chipped area at each point, the area relationship has been used. Quantifying the chipping away of the material may be important when machining to a very high precision is required.

1.4.2 Repeat loading-unloading experiments

As stated earlier, multiple loading-unloading tests were performed to clearly relate the acoustic emission activity to the fracture process. It is conceivable

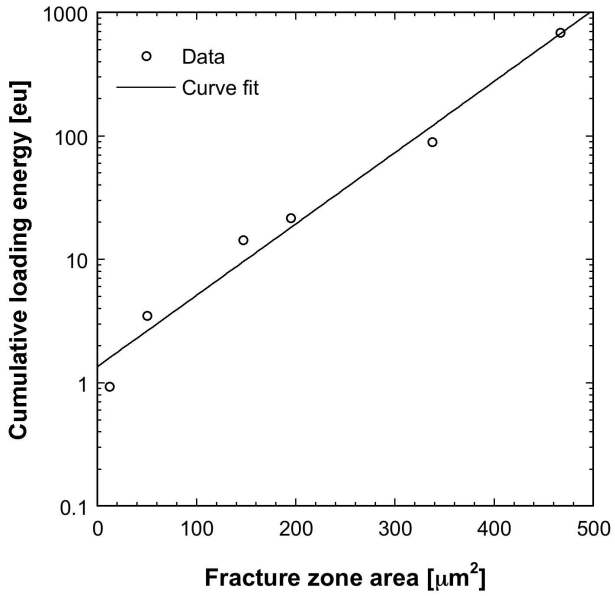

Figure 13: Cumulative acoustic emission energy during loading (log scale) in Macor.

that friction/slipping along the indenter faces could also lead to the generation of acoustic emissions. The multiple loading-unloading tests served as a test to ensure that acoustic emission activity during an experiment corresponds only to fracture and no other spurious events. Fig. 14 shows the results of a typical repeated loading-unloading experiment performed on glass.

No acoustic emission activity was observed during the first cycle in which the maximum load was 25 mN, as this was below the threshold load for glass. Normal acoustic emission was observed in the second cycle in which a maximum load of 125 mN was applied corresponding to the growth of radial cracks. As the specimen was unloaded and reloaded in the third cycle the acoustic emission did not start until the indention load was almost the same as that of the previous maximum load, i.e. 125 mN. This confirmed the fact that no acoustic emissions were detected while the specimen was simply elastically deformed with no accompanying crack growth.

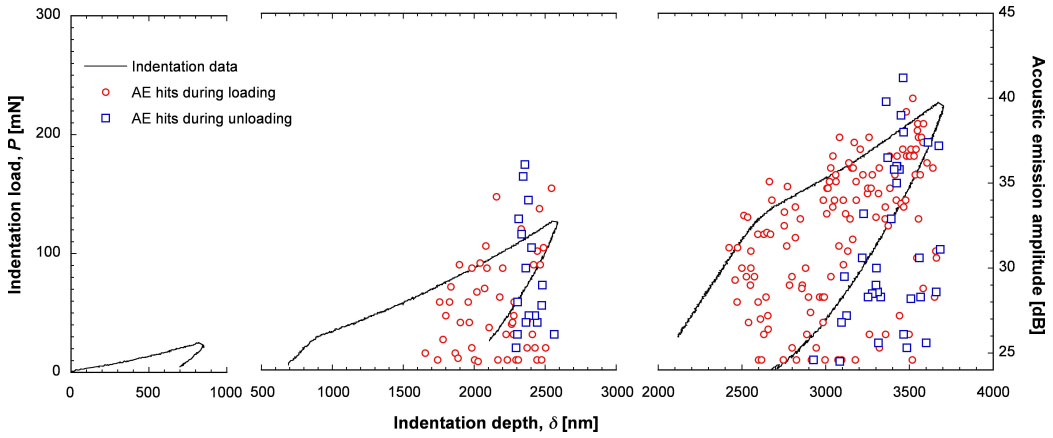

Figure 14: Repeated load and unload experiment on glass for 25mN, 125mN and 225mN load.

1.5 Conclusions

A nanoindentation instrument was successfully retrofitted with a standalone acoustic monitoring system. The real-time monitoring of acoustic emission was then used as a qualitative and quantitative diagnostic tool for investigating indentation induced failure. Three types of materials of varying microstructure were tested; soda lime glass, silicon carbide and Macor. The soda lime glass was chosen as it represents a brittle material with a glassy/amorphous microstructure; beta crystalline silicon carbide offered a more complex material with a face centered cubic polycrystalline microstructure; and the machinable glass ceramic Macor offered a completely different microstructure as a heterogeneous composite with mica reinforcements. Acoustic emission activity was an excellent indicator of fracture even in those cases that did not show any sudden changes in the indentation loading/unloading curve. The occurrence of crack in all cases was confirmed using post-test imaging of the indentation sites using SEM. Besides the identification of the occurrence of failure events, acoustic emission was also used to characterize different types of fracture processes and to quantify specific fracture events. It is shown that the threshold load for the onset of the acoustic activity is unique for each material, and can be used as an indicator of the fracture toughness of the material provided that long radial cracks are formed during the indentation process. The three materials exhibited different fracture mechanisms, due to the differences in the microstructure. This

was reflected in the nature of acoustic emission activity. For glass and silicon carbide the analysis of the loading and unloading acoustic emission energy yielded direct correlations with the radial crack length and wing crack area respectively. This implies that the loading segment of the indentation process leads to radial cracks and the unloading segment leads to wing crack. While, such failure behavior has been postulated in the past, this is one of the few experiments to provide direct experimental evidence. For glass, after the indentation threshold load was reached during loading, the amplitudes of acoustic emission signals increased continuously in proportion to the indentation load. The increasing amplitudes of the acoustic emission may be directly proportional to the surface area of the propagating crack. Upon unloading the amplitude of the acoustic emission signal was higher in comparison to that of loading since considerably more fracture surface area is created through the formation of the wing crack, rather than the radial crack. For silicon carbide the total number of acoustic emission events was much lower than that for glass and instead of continuous crack formation the acoustic emission signals were highly discrete. The discrete signals, during loading, imply crack growth in short bursts rather than a continuous fashion as for glass. The duration times of the acoustic emission events for silicon carbide are shorter than that of glass further implying the short intermittent crack growth. The acoustic energy in silicon carbide is proportional to the area swept by the radial cracks. The correlation between the acoustic emission energy and radial crack lengths can be used to determine the fracture toughness without using optical means to measure the crack lengths. Since the Macor material, a locally heterogeneous composite, did not exhibit radial cracks the fracture toughness cannot be calculated using this technique. However, the damage in this material can be quantified using the acoustic emission energy. In the fracture process of the Macor there are sudden increases in the indentation depth, which most likely correspond to the material undergoing failure process.

2 Nanoscale viscoelastic characterization of polymers using dynamic nanoindentation

Abstract

A new displacement modulation based dynamic indentation method is demonstrated and shown to be effective for viscoelastic characterization of a glassy polymer. Calibration of the measuring instrument is carried out using a cantilever spring and a spring–dashpot model of the system. Subsequently, dynamic indentation tests are carried out on a bishenol-F based epoxy and the complex modulus measurements are compared with bulk dynamic mechanical analysis (DMA) measurements. Storage modulus values are found to be in good agreement with bulk data but some divergence in the case of loss modulus is observed. The calibration procedure of the measuring instrument is critically examined in view of these observations. Overall, displacement modulation based dynamic indentation is shown to be a promising method for viscoelastic characterization at the micron length scales.

2.1 Introduction

The unique properties of polymers and the versatility of their processing methods make them, for many applications, the most sought after materials today. On the other hand, the testing of polymers is complicated because of the fact that their properties are significantly rate and temperature dependent. Traditional methods of testing polymers include creep, stress relaxation and dynamic mechanical analysis (DMA). The increasing use of polymers in MEMS, thin films and nanoscale structures, and the use of surface modified polymers, has resulted in a need for testing methods at small length scales.

In recent years, instrumented indentation has become a popular technique for measuring the mechanical properties of solids at small length scales [18]. The methods for determining the elastic modulus and hardness have become fairly standard and rely on the fact that the displacements recovered during unloading are largely elastic, in which case the elastic punch theory can be used to determine the modulus from the unloading part of the load-displacement data. This method, when applied to polymers, leads to an overestimation of the elastic modulus [19]. Although some correction procedures have been suggested to obtain a better estimate [19, 20], the elastic

modulus alone does not provide a complete representation of the time dependent rheological properties of polymers. Thus indentation analogues of creep, stress relaxation and dynamic mechanical analysis (DMA) have been actively pursued and applied to determine viscoelastic properties at the micro and nano length scales.

Dynamic indentation, which is analogous to DMA, has recieved a lot of attention from researchers in the past few years. The properties that can be obtained are frequency and temperature dependent storage and loss modulus, the loss tangent, tan δ, the glass transition temperature, T_g, the mechanical relaxation and the activation energy for the relaxation process. Also, the application of time-temperature superposition is very easily accomplished on the frequency domain to extend the range of frequencies as demonstrated by Hayes *et al.* [21]. With dynamic indentation, results can be obtained faster and over a wide range of frequencies and the variation of properties can also be obtained as a function of depth. Moreover, the loss tangent, which can be obtained using this technique, has been considered by many as a measure of the degree of viscoelasticity of a material. It not only provides an estimate of damping and viscous energy losses in a material, but can give valuable information about the transition temperatures and the associated activation energies. Thus dynamic indentation can be very useful in characterizing the viscoelastic properties of polymers, polymer coatings and surface modified polymers. It can also be used to determine the variation of viscoelastic properties in heterogenous materials like polymer composites and biological tissues. Finally, apart from determining viscoelastic properties, dynamic indentation can also find applications in characterization of dynamic contacts in MEMS and in several contact processes like dry friction, abrasive and erosive wear etc.

The procedure for carrying out dynamic indentation testing involves the application of an oscillating force or displacement signal to the tip-sample contact and the measurement of the resultant output signal as well as the phase difference between the input and output signals. This information is used to obtain the contact stiffness and damping which are then analyzed to determine the viscoelastic properties of the material. The most common approach for carrying out dynamic indentation is a *force modulation* technique where an oscillating signal is superimposed on the quasi-static load and the output displacement and the phase difference are measured [22]. This approach is used by Triboindenter and Triboscope (Hysitron Incorporated, Minneapolis, MN, USA), NanoIndenter XP (Mechanical Tesing and

Simulation (MTS) Systems Corporation, Eden Prairie, MN, USA) and Ultra-Micro Indentation System (UMIS) (Commonwealth Scientific and Industrial Research Organisation (CISRO), Clayton, South Victoria, Australia).

An early description of this technique using the MTS Nanoindenter II was presented by Loubet *et al.* [22] who measured the storage and loss modulus of rubber polyisoprene, with a modulus of less than 400 MPa. Several other researchers [23, 24, 25, 26] have used this technique and it has been shown to provide viscoelastic properties that are in reasonable agreement with bulk DMA measurements [23, 24, 25]. Most recently, White and Van-Landingham *et al.* [27] have tested four polymers, a cured epoxy, PMMA and two PDMS samples with different crosslink densities using the MTS Nanoindenter. They obtained good agreement between the nanoindentation and bulk rheological data for glassy polymers but more divergent results for the two PDMS samples. They have discussed some significant issues involved in carrying out dynamic indentation like instrument calibration, high strains associated with sharp indenters and the validity of the working equations.

A brief review of the derivation of the working equations is provided here for the discussion of some critical issues in dynamic testing. Sneddon's analysis [28] for a rigid flat punch leads to a simple relation between P and h of the form,

$$P = \frac{4\mu a}{1-\nu} h, \tag{5}$$

where a is the radius of the punch, μ is the shear modulus, and ν is the poisson's ratio. Noting that the area of the contact circle is $A = \pi a^2$ and the shear modulus can be related to elastic modulus through $E = 2\mu(1+\nu)$, differentiating P with respect to h leads to,

$$\frac{dP}{dh} = 2\sqrt{\frac{A}{\pi}} \frac{E}{1-\nu^2}. \tag{6}$$

Using the method of functional equations proposed by Radok [29], which has been shown to be valid for the case of a non-decreasing contact area, we can obtain a solution for the complex modulus by replacing the elastic parameters with viscoelastic parameters to obtain the following expression,

$$\frac{dP^*}{dh} = 2\sqrt{\frac{A}{\pi}} \frac{E^*}{1-\nu^2}. \tag{7}$$

For a hold period, the complex stiffness, dP/dh^*, can be written in terms of

the superimposed oscillating force and displacement signals as,

$$\frac{dP^*}{dh} = \frac{P_0 e^{i\delta}}{h_0}, \tag{8}$$

where the oscillating force and displacement signals are,

$$\Delta P = P_0 e^{i(\omega t+\delta)}, \qquad \Delta h = h_0 e^{i(\omega t)}. \tag{9}$$

Using Eqns. 7 and 8, an expression for the complex modulus can be written as,

$$\frac{E^*}{1-\nu^2} = \frac{1}{2}\sqrt{\frac{\pi}{A}}\,\frac{P_0 e^{i\delta}}{h_0}, \tag{10}$$

or in terms of the reduced complex modulus as,

$$E_r{}^* = \frac{1}{2}\sqrt{\frac{\pi}{A}}\,\frac{P_0 e^{i\delta}}{h_0}. \tag{11}$$

If the dynamic contact stiffness, S, and the dynamic contact damping, C, are known then the complex stiffness can be written as,

$$\frac{dP^*}{dh} = S + iC\omega, \tag{12}$$

and the reduced complex modulus can then be written as

$$E_r{}^* = \frac{1}{2}\sqrt{\frac{\pi}{A}}(S + iC\omega). \tag{13}$$

The above analysis, although strictly true only for a flat punch indenter can be extended to sharp indenters. Pharr and Oliver [30] have shown the relation in Eqn. 6, which is the basis of the above derivation, to be true even in the case of a punch of an arbitrary shape in case of unloading. For a viscoelastic contact, during a hold period, the contact area gradually increases and the oscillations take place along the unloading curve. Moreover, the oscillation amplitude is significantly smaller than the indentation depth. Thus it is reasonable to assume that the analysis for a flat punch as shown above can be extended to a punch of an arbitrary shape for complex modulus measurements.

The contact area A, required in Eqn. 13, can be calculated from the contact depth, h_c, by assuming a shape function of the indenter, i.e.,

$$A = f(h_c), \qquad h_c = h_{max} - \epsilon \frac{P_{max}}{dP/dh}. \tag{14}$$

The use of initial unloading slope to calculate the contact depth as in the above equation is known to give an overestimation for a viscoelastic material. Alternative procedures for calculating the contact depth for viscoelastic contacts from the initial section of the unloading curve have been suggested by Tang *et al.* [20]. But for the purpose of this study on epoxy, it was found that the contact depth can be approximated to a good degree of accuracy by the actual depth of penetration of the indenter into the material.

The high strains associated with a Berkovich indenter are a problem during the loading of the indenter into the material, but the unloading part is free from such problems and the unloading curve is known to provide good values of material properties for elastic materials. Thus it is safe to assume that we can extract linear viscoelastic properties also from the unloading curve. In this study, the hold period is used for dynamic measurements and as discussed earlier, oscillations of the indenter on the material surface take place along the unloading curve. Thus dynamic indentation is a very effective technique for viscoelastic characterization. This is further supported by the excellent results obtained by various researchers using dynamic indentation.

This paper describes a new *displacement modulation* based dynamic indentation method which is in contrast to the *force modulation* methods as it provides the excitation not through the force transducer but through controlled specimen oscillation. This allows the control of amplitude and frequency of excitation independently from the electromagnetic loading coil, potentially making available a wider range of amplitudes and frequencies of excitation that can be applied during indentation. A general description of the technique has also been presented elsewhere [31]. The tests are carried out on the NanoTest Platform (MicroMaterials Ltd., Wrexham, UK) which has a unique pendulum design and a special module for performing dynamic indentation. Calibration of the instrument for dynamic indentation tests is carried out and dynamic indentation tests are performed on an epoxy sample and the results are compared with data from standard DMA tests.

2.2 Displacement modulation based dynamic indentation

2.2.1 Experimental setup

The instrumented indentation setup shown in Fig. 15 has a unique pendulum design, with the pendulum pivoted at approximately midpoint. The load is applied through an electromagnetic transducer at the top of the pendulum and is transferred to the other end, which has the indenter in contact with the sample. Fixed to the bottom of the pendulum is an optically flat glass plate placed parallel to another glass plate mounted on the machine frame. The glass plate mounted on the frame is movable and can be used to adjust the gap between the two plates, allowing control over the system damping. The specimen is mounted on a holder, which has a piezoelectric crystal that provides the oscillation.

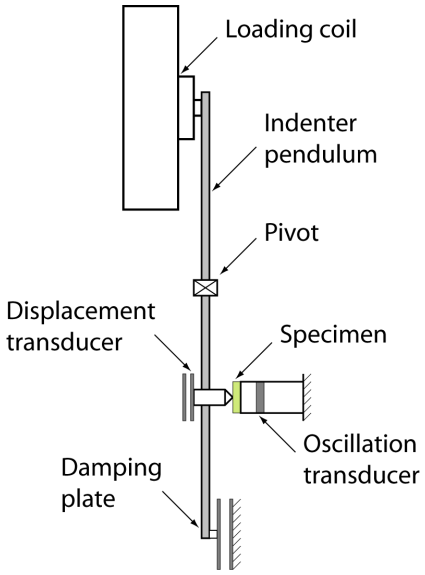

Figure 15: NanoTest setup

A lock-in amplifier signal generator provides the drive signal for sample oscillation. The sample is oscillated at a particular frequency and the displacement signal obtained from the capacitor mounted at the back of the indenter is detected at the same frequency. The capacitor is a part of a bridge circuit. The output from the bridge circuit is amplified and rectified

and then fed back into the lock-in amplifier. The phase difference between the sample oscillation and the pendulum motion is related to the elastic and damping properties of the contact.

2.2.2 Calibration of the setup

The techniques for measuring the dynamic properties in general measure the damping and stiffness characteristics of the indenter-sample contacts as a function of excitation frequency. The damping and stiffness of the contact has to be extracted from the overall response of the system which includes the response of the sample and the machine. Thus it is essential to obtain the measuring instrument's response as a function of excitation frequency. The issue of calibration for quasi-static testing has received a lot of attention in areas like diamond area function (DAF) calibration [32] and machine compliance calibration [33]. A paper by McCormick [34] describes the entire procedure for calibrating a nanoindentation instrument. This effort in the calibration of indentation instruments for the case of quasi-static indentation has contributed to the confidence that we have in quasi-static testing.

A similar effort is required for the understanding of the system characteristics, especially the system damping, for carrying out dynamic experiments. Most of the studies till now have assumed the system damping to be independent of the harmonic frequency. Moreover, in most studies, all the damping elements present in the system have been lumped into one damping parameter. Regardless of the form of the testing instrument, it has a capacitive transducer for measuring displacements and a loading coil for applying a load. These two elements contribute significantly to the system damping in the form of squeeze film and eddy current damping. Both of these damping elements are known to exhibit some sort of frequency dependence, either linear or quadratic. Experimental investigation of these phenomena is not only relevant for the calibration of the indentation instrument but also for other areas like MEMS where they significantly affect device behavior. In this study, a method for extracting the system damping using a cantilever spring and a spring dashpot model of the system is described.

Model and analysis for calibration of setup A spring-dashpot model of the system with a calibration spring in place is shown in Fig. 16. The problem to be solved is analogous to a forced harmonic motion in which an oscillatory displacement is applied to the spring rather than the mass. The

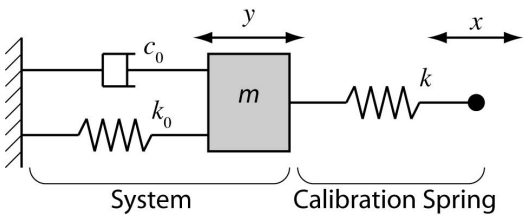

Figure 16: Calibration spring model

equation of motion is given as,

$$m\frac{d^2y}{dt} + c_0\frac{dy}{dt} + k_0 y = 0. \tag{15}$$

where x is the oscillatory displacement applied directly to the sample holder and y is the oscillatory displacement response of the pendulum. Also, m is the system mass, c_0 is the system damping, k_0 is the stiffness of the pendulum springs, and k is the variable stiffness of the calibration spring. The input and output displacements are given as,

$$x = X_0\cos(\omega t), \qquad y = Y_0\cos(\omega t + \phi), \tag{16}$$

where, ω is the excitation frequency and ϕ is the phase difference between the input and output signals. Solving Eqns. 15 and 16 gives the phase difference in terms of the frequency as,

$$\phi = \arctan[\frac{\omega c_0}{k_0 + k - m\omega^2}]. \tag{17}$$

The system electronics introduce a phase offset, ϕ_0, which results in a modification of the above equation as shown below,

$$\phi = \arctan[\frac{\omega c_0}{k_0 + k - m\omega^2}] + \phi_0. \tag{18}$$

Calibration procedure with a cantilevered spring Calibration of the indentation instrument requires the determination of the three system parameters, viz., the electronics phase offset, ϕ_0, the effective pendulum mass, m, and the effective system damping, c_0. To obtain the system parameters, a cantilever calibration spring mounted on the oscillating sample holder was employed as shown in Fig. 17. The spring was made of copper and had a

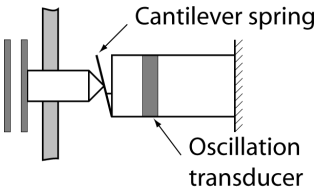

Figure 17: Schematic of the calibration setup with cantilever spring

thickness of 0.14 mm and a width of 1.17 mm. First, the mass of the system was determined by measuring the resonance frequency of the pendulum in contact with the spring at one position along the length of the spring. This provided an effective pendulum mass value of 0.209 kg. The system offset, ϕ_0, was determined by measuring the phase difference between the input and output signals as a function of frequency with a hard contact between the oscillating sample holder and the pendulum. The hard contact was achieved by soldering a brass pin between the indenter holder and the sample holder. Phase offset measurements were carried out for two damping plate spacings of 140 μm and 360 μm corresponding to high and low damping. The results are shown in Fig. 18 and indicate that the system offset is independent of the system damping. To determine the system damping, oscillation data

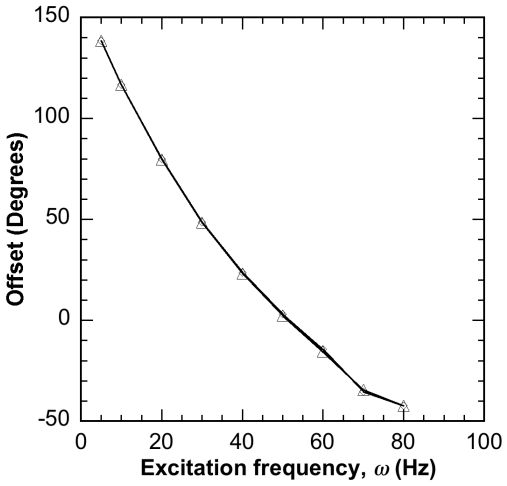

Figure 18: System damping as a function of harmonic frequency

was acquired at different positions along the length of the spring. At each

position, the phase difference between the input and output signals as well as the stiffness of the spring was recorded. Phase difference was recorded by the Lock-in amplifier and the spring stiffness was determined by carrying out load ramp tests with the indenter in contact with the spring at the given point. The experimentally determined values of spring stiffness were within 1% of theoretical calculations. Thus at each position, phase as well as the compliance of the spring are known. Since the system mass and system phase offset are already known using independent methods, damping being the only unknown can be calculated using Eqn. 18. Damping values calculated as a function of spring compliance are shown in Fig. 19 for one of the frequencies, 20 Hz.

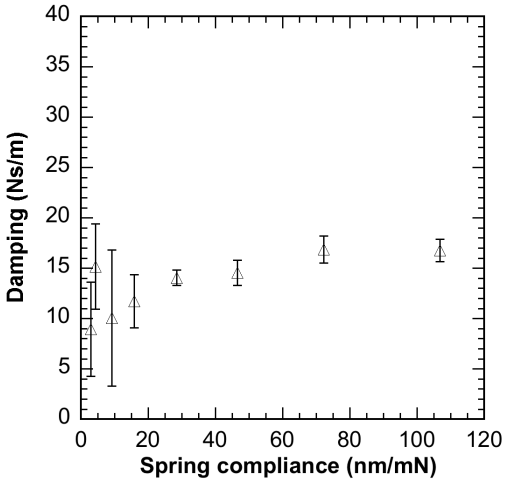

Figure 19: System damping as a function of spring compliance for 20 Hz

To obtain the system damping at 20 Hz, an average of the values for all the compliances was taken. The system damping values obtained using the above method for the frequencies of 10, 20 and 40 Hz are shown in Fig. 20. These system damping values are used during the analysis of the dynamic indentation experiments on a polymer sample as described in the following section.

2.2.3 Measurement of complex modulus

Model A spring-dashpot model of the material-indenter interaction with a contact stiffness, k', and a contact damping, c', in parallel is assumed.

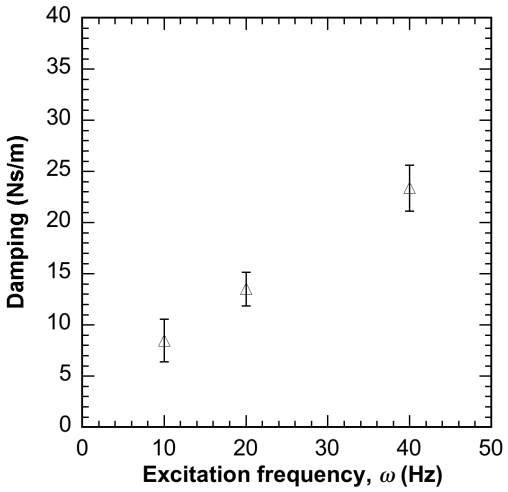

Figure 20: System damping as a function of harmonic frequency

The governing equation of the system with the sample in place is similar to Eqn. 18, but with additional damping and stiffness terms included to account for the contact damping and stiffness,

$$\phi = \arctan[\frac{\omega(c_0 + c')}{k_0 + k' - m\omega^2}] + \phi_0. \tag{19}$$

Both c' and k' are assumed to be frequency dependent. Also, it is known that the contact stiffness k' is proportional to the square root of the contact area, i.e., to x for a perfectly pyramidal indenter. The contact damping is also assumed to be proportional to depth, since this assumption leads to a loss modulus value that is independent of depth. Thus Eqn. 19 is written as,

$$\phi = \arctan[\frac{\omega(c_0 + cx)}{k_0 + kx - m\omega^2}] + \phi_0, \tag{20}$$

where x is the contact depth and c and k are constants. For the measurement of complex modulus, a set of load-partial unload indentations is produced, with the phase angle being measured during the dwell period. The contact depth is usually found from the unloading curve using the Oliver-Pharr analysis [35] assuming elastic deformation. But this procedure is known to give erroneous results for viscoelastic materials. Alternative procedures for calculating the contact depth for viscoelastic contacts from the initial section

of the unloading curve have been suggested by Tang *et al.* [20]. But for the purpose of this study on epoxy it was found that the contact depth can be approximated to a good degree of accuracy by the actual depth of penetration of the indenter into the material. Finally, since m and c_0 are known from the calibration procedure, fitting the phase versus depth data allows c and k to be determined. The storage modulus, E' , and the loss modulus, E'' , can then be calculated using Eqn. 13 as,

$$E' = \frac{k}{2}\sqrt{\frac{\pi}{24.5}}, \tag{21}$$

$$E'' = \frac{c\omega}{2}\sqrt{\frac{\pi}{24.5}}. \tag{22}$$

An ideal Berkovich geometry was assumed because it was found that for plastic depths beyond 400 nm, the diamond area function does not have a significant effect on the analysis.

Material and experiments Using the above method, complex modulus measurements were carried out on a thermosetting epoxy sample. The epoxy resin chosen for this study, EPON Resin 862 (Resolution Performance Products, Houston, Texas, USA), is a low-viscosity liquid epoxy resin manufactured from epichlorohydrin and bisphenol-F. It is a typical highly crosslinked thermosetting polymer that exhibits brittle behavior, and has the ideal structural formula as shown in Fig. 21. A moderately reactive, low viscosity

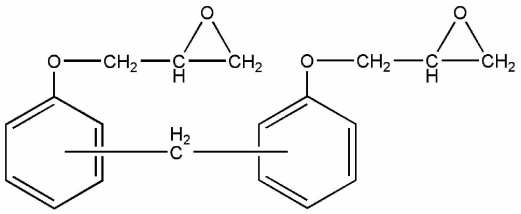

Figure 21: Structural formula of the epoxy resin used in this study

aliphatic amine, EPIKURE 3274 (Resolution Performance Products, Houston, Texas, USA) was used as the curing agent. This curing agent provides a pot life of about 1 hour after mixing, which was required to remove the air bubbles trapped in the mixture before making the final cast. Properties of

Property	EPON Resin 862
Manufacturer	Resolution performance products
Curing agent	Epikure 3274 (low viscosity aliphatic amine)
Curing cycle	24 hours at 25C; 6 hours at 120C
Young's Modulus	3.24 GPa
Fracture Toughness	1.11 MPa.$m^{1/2}$
Density	1230 kg/m^3

Table 4: Nominal bulk properties of the epoxy used in this study

neat EPON 862 resin cured with the EPIKURE 3234 curing agent are listed in Table 4.

The indentation samples were cut in the form of small tablets with nominal dimensions of 10 x 10 x 5 mm. The testing surface was polished on a metallographic polishing wheel using 0.05 μm diamond polishing suspension. Then the samples were mounted onto the sample holder using a cyanoacrylate based superglue and dynamic indentation tests were carried out at the frequencies of 10, 20 and 40 Hz. Figure 22 shows the variation of the experimental phase values, ϕ, as a function of the plastic depth x. Curvefit of this data with the theoretical spring-dashpot model as per Eqn. 20, provides the contact stiffness and the contact damping. The model curvefits are also shown in Fig. 22 for each frequency. The contact stiffness and damping values were then used to obtain the storage and loss moduli using Eqns. 21 and 22. Figure 23 shows the variation of the storage and loss moduli, determined using dynamic indentation, as a function of testing frequency, along with the bulk moduli obtained using dynamic mechanical analysis (DMA) tests. The DMA tests were carried out on a Tritec 2000 DMA machine (Triton Technology Ltd., Keyworth, UK) which provides data up to a maximum testing frequency of 20 Hz. Comparison of the two results shows that the storage modulus values obtained using dynamic indentation are in very good agreement with those from DMA but there is some discrepancy in the loss modulus. The good agreement of the storage modulus values indicates the effectiveness of the technique and justifies further application. On the other hand, the discrepancy in the loss modulus values requires further investigation. The loss modulus values obtained using dynamic indentation are extremely sensitive to the system damping. Thus a critical examination of the system damping calibration procedure is required.

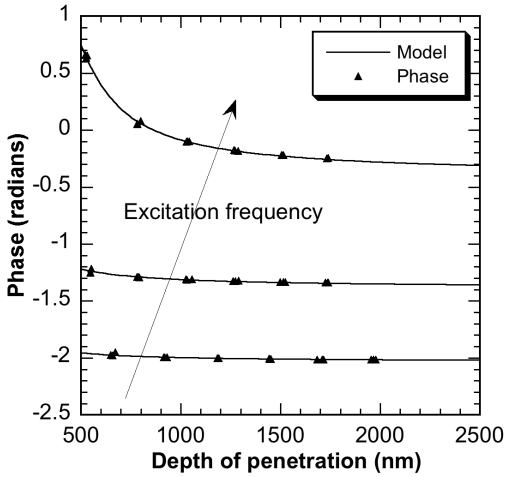

Figure 22: Experimental phase values and curvefits for epoxy

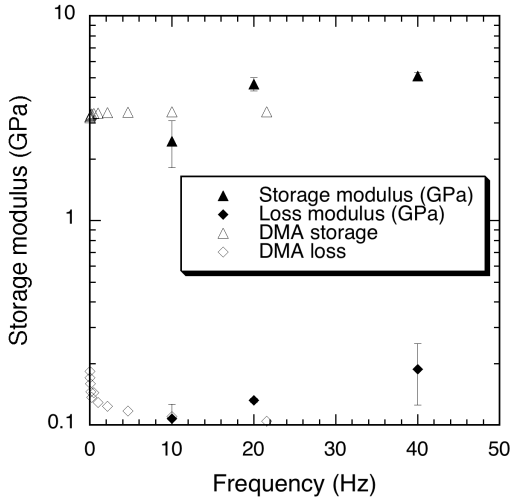

Figure 23: Storage and loss modulus obtained from curvefit and DMA

2.2.4 Issues in calibration procedure using a cantilevered spring

Measurement of the loss modulus using dynamic indentation requires the measurement of contact damping, which in turn is very sensitive to the accuracy of system damping measurements. The mismatch between the loss modulus values obtained from dynamic indentation and those from DMA, necessitates a critical evaluation of the calibration procedure described in section 2.2. The calibration was carried out using a cantilevered spring that was loaded in contact with the indenter. This doesn't rule out a possibility of slipping of the indenter on the spring during oscillation resulting in a scatter in the data. This scatter would affect the determination of system damping parameters. There is a need to eliminate this problem by using a configuration that employs a direct bond or connection between the indenter stub and the spring. Furthermore, a spring-dashpot model has been used and all the damping elements have been lumped together into a single damping parameter. The system damping in the NanoTest is believed to be contributed by three elements, squeeze film damping between the damping plates, the squeeze film damping between the capacitor plates, and the eddy current damping in the loading coil. The use of a single damping parameter may not be an accurate representation of the system characteristics and a better model of the system is required.

2.3 Summary

With the increasing use of polymers and polymer composites in MEMS and in nanotechnology, the need for experimental methods to measure viscoelasticity at the micro and nanoscale is expanding. Instrumented indentation has been very successful for characterizing elastic properties at these length scales. But the testing of viscoelastic properties like creep and stress relaxation has proved a challenge although some progress has been made in recent years. Dynamic indentation offers several advantages over quasi-static indentation methods for viscoelastic characterization including faster testing times and easier analysis procedures. A new displacement modulation based dynamic indentation method has been developed and demonstrated in this paper. In this technique, oscillation is provided through controlled sample oscillation rather than through the force transducer as is done in the case of force modulation methods. Extraction of the material properties requires the analysis of the overall response of the system, which includes the response

of the machine as a function of frequency. Thus it is essential to obtain the measuring instrument's response, especially damping, as a function of excitation frequency. A simple spring-dashpot model has been used to obtain the system damping using a calibration spring and phase measurements. These damping values have been used to analyze dynamic experiments on polymers using the phase measurements over a range of frequencies. The good agreement between the storage modulus values from dynamic indentation and bulk DMA tests indicates the effectiveness of the technique and excellent scope for further applications. Some discrepancy between the loss modulus values obtained using this method and those from DMA tests has been observed. This is attributed to the uncertainities in the system damping measurements and requires further investigation.

References

[1] Doener, M., and Nix, W., 1986. "A Method for Interpreting the Data from Depth-Sensing Indentation Instruments". *Journal of Materials Research,* **1**, pp. 601–609.

[2] Oliver, W. C., and Pharr, G. M., 1992. "An Improved Technique for Determining Hardness and Elastic-Modulus Using Load and Displacement Sensing Indentation Experiments". *Journal of Materials Research J. Mater. Res.,* **7**(6), pp. 1564–1583.

[3] Pharr, G. M., 1998. "Measurement of mechanical properties by ultra-low load indentation". *Materials Science and Engineering a-Structural Materials Properties Microstructure and Processing Mater. Sci. Eng. A-Struct. Mater. Prop. Microstruct. Process.,* **253**(1-2), pp. 151–159.

[4] Harding, D., Oliver, W., and Pharr, G., 1995. "Cracking during nanoindentation and its use in the measurement of fracture toughness". *Proceedings of the 1994 Fall Meeting of MRS. 1995,* **356**, pp. 663–668.

[5] Lawn, B. R., Evans, A. G., and Marshall, D. B., 1980. "Elastic-Plastic Indentation Damage in Ceramics - the Median-Radial Crack System". *Journal of the American Ceramic Society J. Am. Ceram. Soc.,* **63**(9-10), pp. 574–581.

[6] Bohse, J., 2000. "Acoustic emission characteristics of micro-failure processes in polymer blends and composites". *Composites Science and Technology,* **60**(8), pp. 1213–1226.

[7] Daugela, A., Kutomi, H., and Wyrobek, T., 2001. "Nanoindentation induced acoustic emission monitoring of native oxide fracture and phase transformations". *Zeitschrift fuer Metallkunde/Materials Research and Advanced Techniques,* **92**(9), pp. 1052–1056.

[8] Tymiak, N. I., Daugela, A., Wyrobek, T. J., and Warren, O. L., 2003. "Highly localized acoustic emission monitoring of nanoscale indentation contacts". *Journal of Materials Research,* **18**(4), pp. 784–796.

[9] Hay, J. L., and Pharr, G. M., 2000. *Instrumented Indentation Testing*, Vol. 8.

[10] From, P. S., Pyrz, R., Clausen, B., and Nielsen, E. O., 1995. "Indentation and Acoustic-Emission in Filtration Processed Platelet Reinforced Ceramics". *Materials Science and Engineering a-Structural Materials Properties Microstructure and Processing,* **197**(2), pp. 231–236.

[11] Mader, E., Moos, E., and Karger-Kocsis, J., 2001. "Role of film formers in glass fibre reinforced polypropylene - new insights and relation to mechanical properties". *Composites Part a-Applied Science and Manufacturing,* **32**(5), pp. 631–639.

[12] Ostojic, P., and McPherson, R., 1987. "A Review of Indentation Fracture Theory - Its Development, Principles and Limitations". *International Journal of Fracture Int. J. Fract.,* **33**(4), pp. 297–312.

[13] Yurkov, A. L., Breval, E., and Bradt, R. C., 1996. "Cracking during indentation in Sialon-based ceramics: Kinetic microhardness and acoustic emission". *Journal of Materials Science Letters J. Mater. Sci. Lett.,* **15**(11), pp. 987–990.

[14] Rabiei, A., Enoki, M., and Kishi, T., 2000. "A study on fracture behavior of particle reinforced metal matrix composites by using acoustic emission source characterization". *Materials Science and Engineering a-Structural Materials Properties Microstructure and Processing,* **293**(1-2), pp. 81–87.

[15] Cook, R. F., and Pharr, G. M., 1990. "Direct observation and analysis of indentation cracking in glasses and ceramics". *Journal of the American Ceramic Society,* **73**(4), pp. 787–817.

[16] Gerberich, W., and Hartbower, C., 1967. "Some Observations on Stress Wave Emission as a Measure of Crack Growth". *International Journal of Fracture Mechanics,* **3**(3), pp. 185–&.

[17] Bahr, D., and Gerberich, W., 1998. "Relationships between acoustic emission signals and physical phenomena during indentation". *Journal of Materials Research,* **13**(4), pp. 1065–1074.

[18] Hay, J., and Pharr, G., 2000. "Instrumented Indentation Testing". *ASM Handbook, Volume 8, Mechanical Testing and Evaluation Edited by H. Kuhn and D. Medlin*, pp. 232–243.

[19] Feng, G., and Ngan, A. H. W., 2002. "Effects of creep and thermal drift on modulus measurement using depth-sensing indentation". *Journal of Materials Research,* **17**(3), pp. 660–668.

[20] Tang, B., and Ngan, A. H. W., 2003. "Accurate measurement of tip-sample contact size during nanoindentation of viscoelastic materials". *J. Mater. Res.,* **18**(5), pp. 1141–1148.

[21] Hayes, S., Goruppa, A., and Jones, F., 2004. "Dynamic nanoindentation as a tool for the examination of polymeric materials". *Journal of Materials Research,* **19**(11), pp. 3298 – 3306.

[22] Loubet, J. L., Lucas, B. N., and Oliver, W. C., 1995. "Some measurements of viscoelastic properties with the help of nanoindentation". *National Institute of Standards Special Publication 896. Conference Proceedings: International Workshop on Instrumented Indentation, San Diego*, pp. 31–34.

[23] Loubet, J., Oliver, W., and Lucas, B., 2000. "Measurement of the loss tangent of low-density polyethylene with a nanoindentation technique". *Journal of Materials Research,* **15**(5), pp. 1195 – 1198.

[24] Odegard, G., Gates, T., and Herring, H., 2005. "Characterization of viscoelastic properties of polymeric materials through nanoindentation". *Experimental Mechanics,* **45**(2), pp. 130 – 136.

[25] Asif, S. S., and Pethica, J., 1998. "Nano-scale viscoelastic properties of polymer materials". *Materials Research Society Symposium - Proceedings,* **505**, pp. 103 – 108.

[26] Conte, N., and Jardret, V., 2002. "Frequency specific characterization of very soft polymeric materials using nanoindentation testing". *Materials Research Society Symposium - Proceedings,* **710**, pp. 105 – 110.

[27] White, C., Vanlandingham, M., Drzal, P., Chang, N.-K., and Chang, S.-H., 2005. "Viscoelastic characterization of polymers using instrumented indentation. II. Dynamic testing". *Journal of Polymer Science, Part B: Polymer Physics,* **43**(14), pp. 1812 – 1824.

[28] Sneddon, I. N., 1965. "The relation between load and penetration in the axisymmetric Boussinisque problem for a punch of arbitrary profile". *Int. J. Engng Sci.,* **3**, pp. 47–57.

[29] Radok, J. R. M., 1957. "Visco-elastic stress analysis". *Quarterly of Applied Mathematics,* **15**, pp. 198–202.

[30] Phar, G. M., Oliver, W. C., and Broetzen, F. R., 1992. "On the generality of the relationship among contact stiffness, contact area, and elastic modulus during indentation". *Journal of Materials Research,* **7**(3), pp. 613–617.

[31] Singh, S. P., Singh, R. P., and Smith, J. F., 2005. "Displacement modulation based dynamic nanoindentation for viscoelastic material characterization". *Materials Research Society Symposium Proceedings*, pp. 141 – 146.

[32] Herrmann, K., Jennett, N., Wegener, W., Meneve, J., Hasche, K., and Seemann, R., 2000. "Progress in determination of the area function of indenters used for nanoindentation". *Thin Solid Films,* **377-378**, pp. 394 – 400.

[33] Sun, Y., Zheng, S., Bell, T., and Smith, J., 1999. "Indenter tip radius and load frame compliance calibration using nanoindentation loading curves". *Philosophical Magazine Letters,* **79**(9), pp. 649 – 658.

[34] McCormick, N., Gee, M., and Hall, D., 1993. "Calibration of the nanoindenter". *Materials Research Society Symposium Proceedings,* **308**, pp. 195 – 200.

[35] Oliver, W., and Pharr, G., 1992. "Improved technique for determining hardness and elastic modulus using load and displacement sensing indentation experiments". *Journal of Materials Research,* **7**(6), pp. 1564–1580.